093391
(24)

ELSEVIER

Journal of Volcanology and Geothermal Research 107 (2001) 241–264

Journal of volcanology and geothermal research

www.elsevier.com/locate/jvolgeores

Effusive eruptions from a large silicic magma chamber: the Bearhead Rhyolite, Jemez volcanic field, NM

Leigh Justet*, Terry L. Spell

Department of Geosciences, University of Nevada, Las Vegas, NV 89154-4010, USA

Received 23 February 2000; accepted 6 November 2000

Abstract

Large continental silicic magma systems commonly produce voluminous ignimbrites and associated caldera collapse events. Less conspicuous and relatively poorly documented are cases in which silicic magma chambers of similar size to those associated with caldera-forming events produce dominantly effusive eruptions of small-volume rhyolite domes and flows. The Bearhead Rhyolite and associated Peralta Tuff Member in the Jemez volcanic field, New Mexico, represent small-volume eruptions from a large silicic magma system in which no caldera-forming event occurred, and thus may have implications for the genesis and eruption of large volumes of silicic magma and the long-term evolution of continental silicic magma systems.

$^{40}Ar/^{39}Ar$ dating reveals that most units mapped as Bearhead Rhyolite and Peralta Tuff (the Main Group) were erupted during an ~540 ka interval between 7.06 and 6.52 Ma. These rocks define a chemically coherent group of high-silica rhyolites that can be related by simple fractional crystallization models. Preceding the Main Group, minor amounts of unrelated trachydacite and low silica rhyolite were erupted at ~11–9 and ~8 Ma, respectively, whereas subsequent to the Main Group minor amounts of unrelated rhyolites were erupted at ~6.1 and ~1.5 Ma.

The chemical coherency, apparent fractional crystallization-derived geochemical trends, large areal distribution of rhyolite domes (~200 km^2), and presence of a major hydrothermal system support the hypothesis that Main Group magmas were derived from a single, large, shallow magma chamber. The ~540 ka eruptive interval demands input of heat into the system by replenishment with silicic melts, or basaltic underplating to maintain the Bearhead Rhyolite magma chamber.

Although the volatile content of Main Group magmas was within the range of rhyolites from major caldera-forming eruptions such as the Bandelier and Bishop Tuffs, eruptions were smaller volume and dominantly effusive. Bearhead Rhyolite domes occur at the intersection of faults, and are cut by faults, suggesting that the magma chamber was structurally vented preventing volatiles from accumulating to levels high enough to trigger a caldera-forming eruption. © 2001 Elsevier Science B.V. All rights reserved.

1. Introduction

The most cataclysmic volcanic eruptions recorded in the geologic record are associated with continental caldera-forming events in which 100–1000's km^3 of silicic magma are rapidly discharged from pluton-sized shallow magma chambers. Due to their conspicuous nature, calderas and associated ignimbrites have been intensely studied. However, there is another style of silicic volcanism that remains poorly documented. This style is characterized by widely distributed silicic domes, flows, and associated small volume pyroclastic deposits that are derived from a

* Corresponding author. Tel.: +1-702-895-4616; fax: +1-702-895-4064.

E-mail address: justet@nevada.edu (L. Justet), tspell@cemail.nevada.edu (T.L. Spell).

0377-0273/01/$ – see front matter © 2001 Elsevier Science B.V. All rights reserved.
PII: S0377-0273(00)00296-1

14362

RECEIVED AUG 14 2006 By

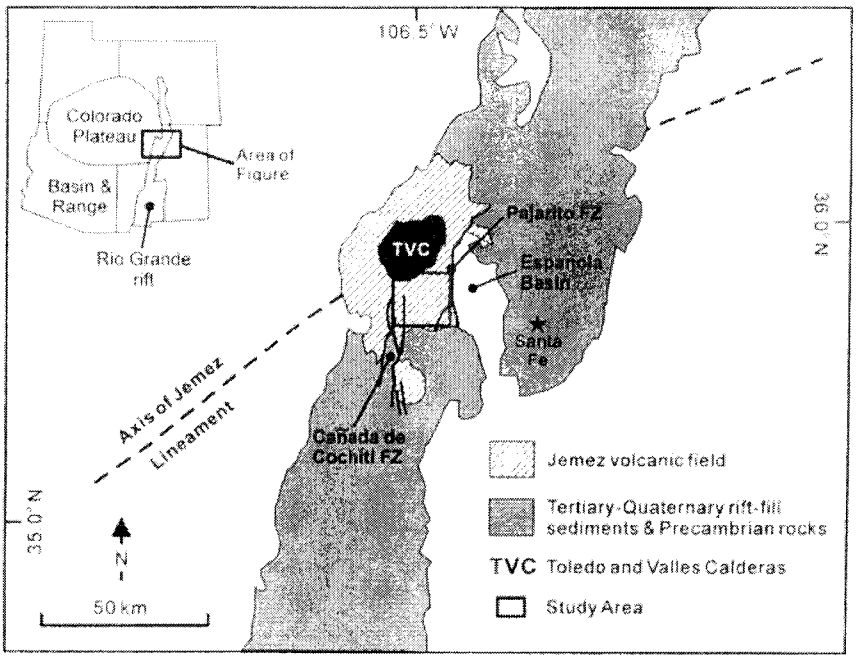

Fig. 1. Regional tectonic map showing the relationship between the Rio Grande rift, Jemez Lineament, and Jemez volcanic field (after Baldridge et al., 1983; Gardner and Goff, 1984; Self et al., 1986). FZ, fault zone.

single large, shallow magma chamber, over intervals of time ranging to 100's ka, without an associated caldera-forming event. Where this eruptive style has been recognized, at Coso volcanic field, CA, (Bacon et al., 1981) and the Taylor Creek Rhyolite, Mogollon–Datil volcanic field, NM (Duffield and du Bray, 1990; Duffield and Dalrymple, 1990), the magma chamber may have been vented along faults before a caldera-forming eruption could occur.

The Bearhead Rhyolite and Peralta Tuff Member from the Jemez volcanic field, NM, represents another example of this eruptive style. Much of the Bearhead Rhyolite and Peralta Tuff apparently was derived from a single large magma chamber similar to the size of those which later produced the Bandelier Tuffs and associated Toledo/Valles calderas at 1.6 and 1.2 Ma. Most of the Bearhead Rhyolite was erupted during a ~540 ka interval, and did not produce a caldera-forming eruption. Like the Coso and Taylor Creek Rhyolite, Bearhead Rhyolite magmas were probably vented by faults related to regional extension along the Rio Grande rift, leading to small-scale, dominantly effusive eruptions despite the presence of a large, shallow, volatile-charged silicic magma chamber.

These rhyolites may represent a style of silicic volcanism that is more common than realized because silicic dome fields are not obviously related to a single event/magma chamber as are calderas and ash flow tuffs. Recognition and study of this eruptive style may lend new insight into understanding the genesis and evolution of large volumes of silicic magma. Our data imply that the style of rhyolitic volcanism early in the development of the Jemez volcanic field differs from the later caldera-forming eruptions of the Bandelier Tuff and thus may have important implications for the long-term evolution of large continental volcanic systems.

2. Geologic setting

The Jemez volcanic field is located at the intersection of the Jemez Lineament and Rio Grande rift in north-central New Mexico (Fig. 1). The Jemez Lineament is a northeast trending array of volcanic centers

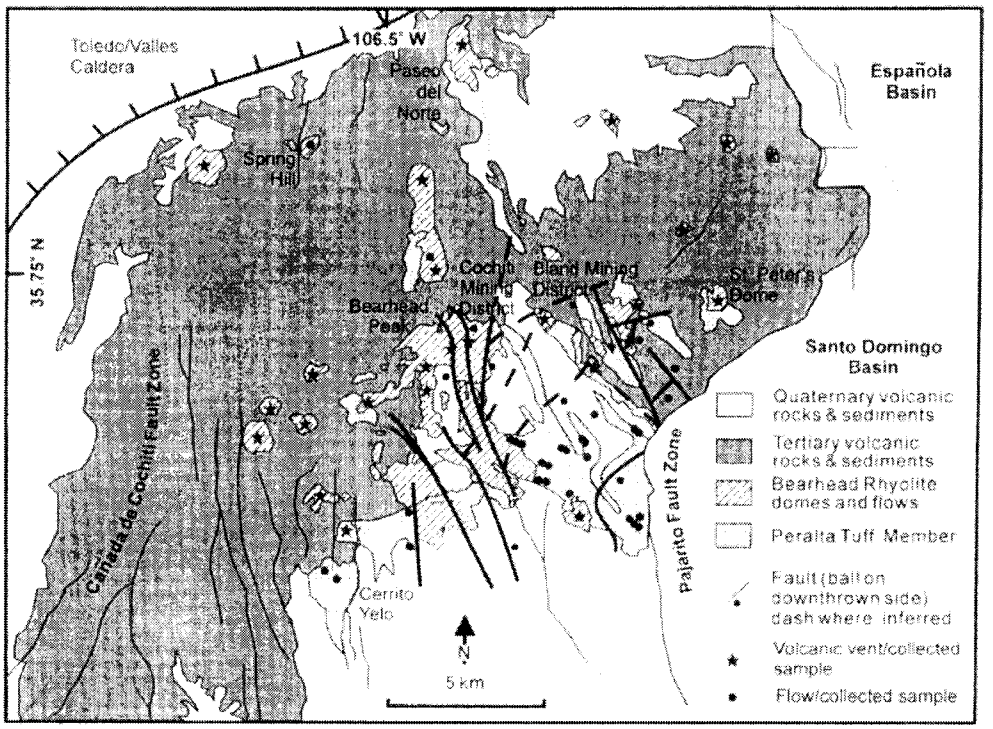

Fig. 2. Structural map of the study area in the south-central Jemez Mountains. Thin fault lines are based on the mapping of Smith et al. (1970). Thick fault lines, based on the mapping of G.A. Smith and Kuhle (unpubl.), depict the geometry of the Bearhead Basin. Map after Smith et al. (1970).

that reaches from southeast Arizona to northeast New Mexico (Smith and Bailey, 1968; Aldrich, 1986). The Rio Grande rift comprises a series of en-echelon sedimentary basins that extend through Upper Paleozoic sedimentary strata and Precambrian basement (Doell et al., 1968; Aldrich, 1986). The Jemez volcanic field lies on the western flank of the Española Basin and is cut by the Cañada de Cochiti and Pajarito fault zones; the west-bounding faults of the Española Basin (Fig. 1).

Volcanic activity in the Jemez volcanic field began around 16.5 Ma (Gardner and Goff, 1984) and continued as recently as ~60 ka (Wolff and Gardner, 1995; Reneau et al., 1996). Keres Group volcanism occurred between 13 and 6 Ma as a series of basalt through high-silica rhyolite eruptions in the southern portion of the volcanic field. High rates of extension along the Rio Grande rift from 13 to 7 Ma coincide with the eruption of large volumes of Keres Group basalt and andesite. Decreased extension around 5 Ma led to a hiatus in mafic and intermediate volcanism (Aldrich, 1986; Self et al., 1986; Gardner and Goff, 1984). The Bearhead Rhyolite and Peralta Tuff were erupted during the waning stages of Keres Group volcanism.

More than 500 km^3 of andesite, dacite, and rhyodacite of the Polvadera Group were erupted between 6.9 and 2.2 Ma (Gardner et al., 1986; Goff et al., 1989). The early stages of volcanism in the north and northeast coincided with the final stages of Keres Group volcanism in the south. An increase in extension around 4–2 Ma was accompanied by eruption of the Basalts of Cerros del Rio, El Alto, and Santa Anna Mesa (Dunker et al., 1991).

These basaltic eruptions were followed by rhyolitic volcanism of the Tewa Group from 1.85 Ma to 60 ka (Izett and Obradovich, 1994; Reneau et al., 1996; Spell et al., 1996). At 1.61 and 1.22 Ma the large-scale Bandelier Tuff eruptions (~700 km^3 total)

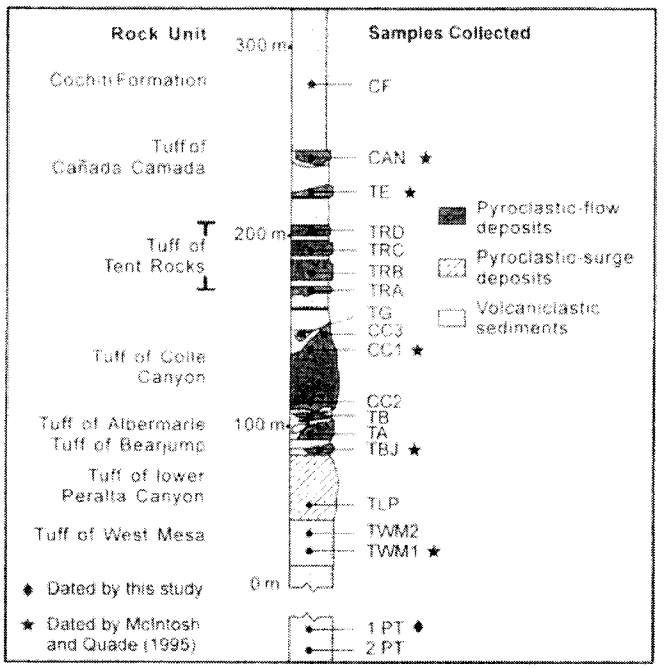

Fig. 3. Stratigraphic column of Peralta Tuff showing samples collected for this study (Gay and Smith, 1996).

produced the Toledo and Valles calderas near the center of the Jemez volcanic field.

3. Overview of the Bearhead Rhyolite and Peralta Tuff

The Bearhead Rhyolite was initially mapped and defined by Smith et al. (1970) as a series of domes, composite domes, and flows. Subsequently, the Bearhead Rhyolite has been mapped in greater detail by Gardner (1985) and Goff et al. (1990). The Bearhead Rhyolite is located in the southeastern portion of the Jemez volcanic field, and extends across an ~200 km^2 area as a series of 26 domes, composite domes, flows, and shallow intrusions (Figs. 1 and 2). The Peralta Tuff Member represents the explosive eruptive phase of Bearhead Rhyolite that consists of small-volume pyroclastic fall and reworked deposits. Gay and Smith (1996) worked out an informal stratigraphy of a ~300 m section of the Peralta Tuff in the southern part of the field area on which this study based its sampling strategy. The Bearhead Rhyolite and Peralta Tuff represent the final stages of silicic volcanism in the Keres Group as well as the last pulse of silicic volcanism before a 2 Ma hiatus throughout the Jemez volcanic field.

The dome field lies at the intersection of the Cañada de Cochiti (to the west) and Pajarito (to the southeast) fault zones (Fig. 2). Most faults in the north-striking Cañada de Cochiti fault zone have a down-to-the-east sense of displacement with >500 m of offset. The Cañada de Cochiti fault zone is thought to have been active during Keres Group volcanism because Keres deposits are cut by these faults and thicken to the east across the fault zone (Gardner, 1985). The Bearhead Rhyolite is commonly intruded along these faults and is locally cut by faults (G. Smith, personal communication). The Pajarito fault zone is characterized by down-to-the-east northeast-striking normal faults (Griggs, 1964; Smith et al., 1970; Golombek, 1981). Gardner (1985) suggested that this segment of the fault zone became active around 5 Ma, implying that the western margin of the Española Basin shifted from the Cañada de Cochiti fault zone to the Pajarito fault zone around 6–5 Ma

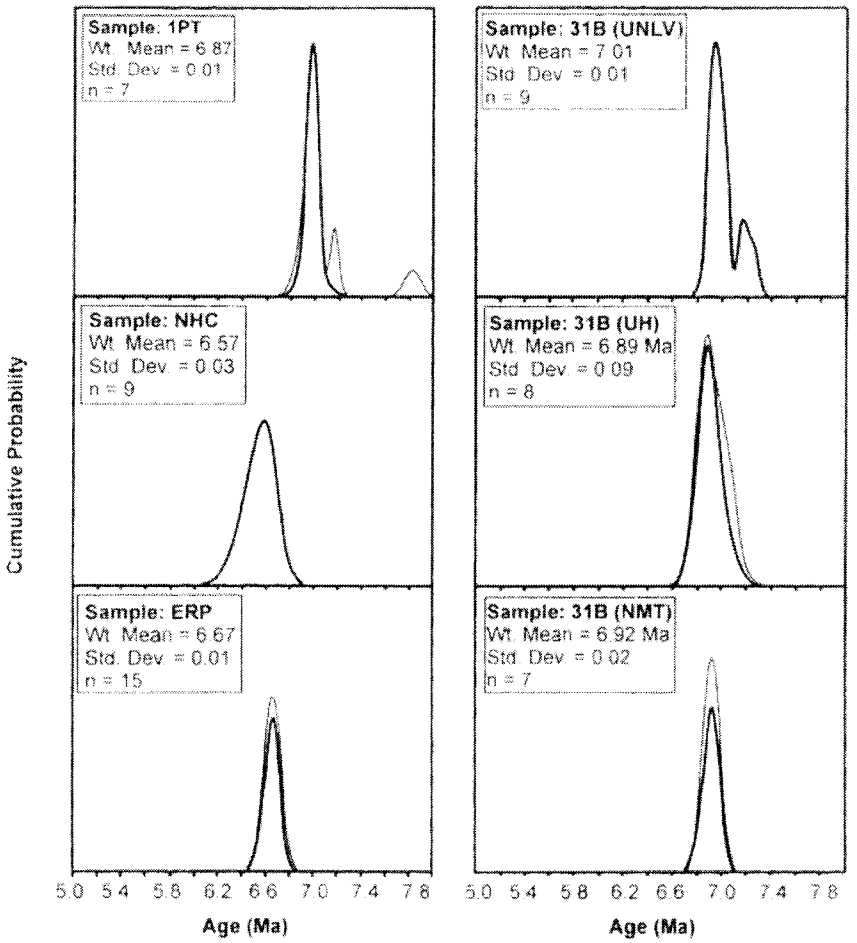

Fig. 4. Representative probability distribution diagrams for single crystal $^{40}Ar/^{39}Ar$ analyses of Bearhead Rhyolite samples. Thick lines denote data that lie within 2σ of the mean sample age and thin lines depict all data. Weighted mean is expressed in Ma.

(see also Manley, 1976, 1979; Golombek, 1981, 1983; Golombek et al., 1983). This shift in faulting coincides with the ~8.1–5.6 Ma hydrothermal alteration event in the Cochiti Mining District (WoldeGabriel and Goff, 1989) (Fig. 2).

The overlapping fault geometries of the Cañada de Cochiti and Pajarito fault zones resulted in rectilinear fault blocks that underwent differential subsidence during late Miocene rhyolitic volcanism (Smith and Kuhle, 1998). The Bearhead Basin, one of these subsidence features, is a west-tilted basin that accumulated at least 700 m of lava, tuff, and coeval volcaniclastic rocks between ~7 and 6.7 Ma (Fig. 2) (Smith and Kuhle, 1998). As a result, most of the Peralta Tuff is preserved in the Bearhead Basin.

4. Analytical methods

Several kilograms of rock were collected at each of 26 domes and four flows mapped as Bearhead Rhyolite by Smith et al. (1970); Gardner (1985), and Goff et al. (1990) as well as ~2000 cm^3 of 19 pumice samples from a ~300 m section of the Peralta Tuff (Fig. 3), for geochemical analysis. Major and trace elements were analyzed by XRF and INAA techniques at the

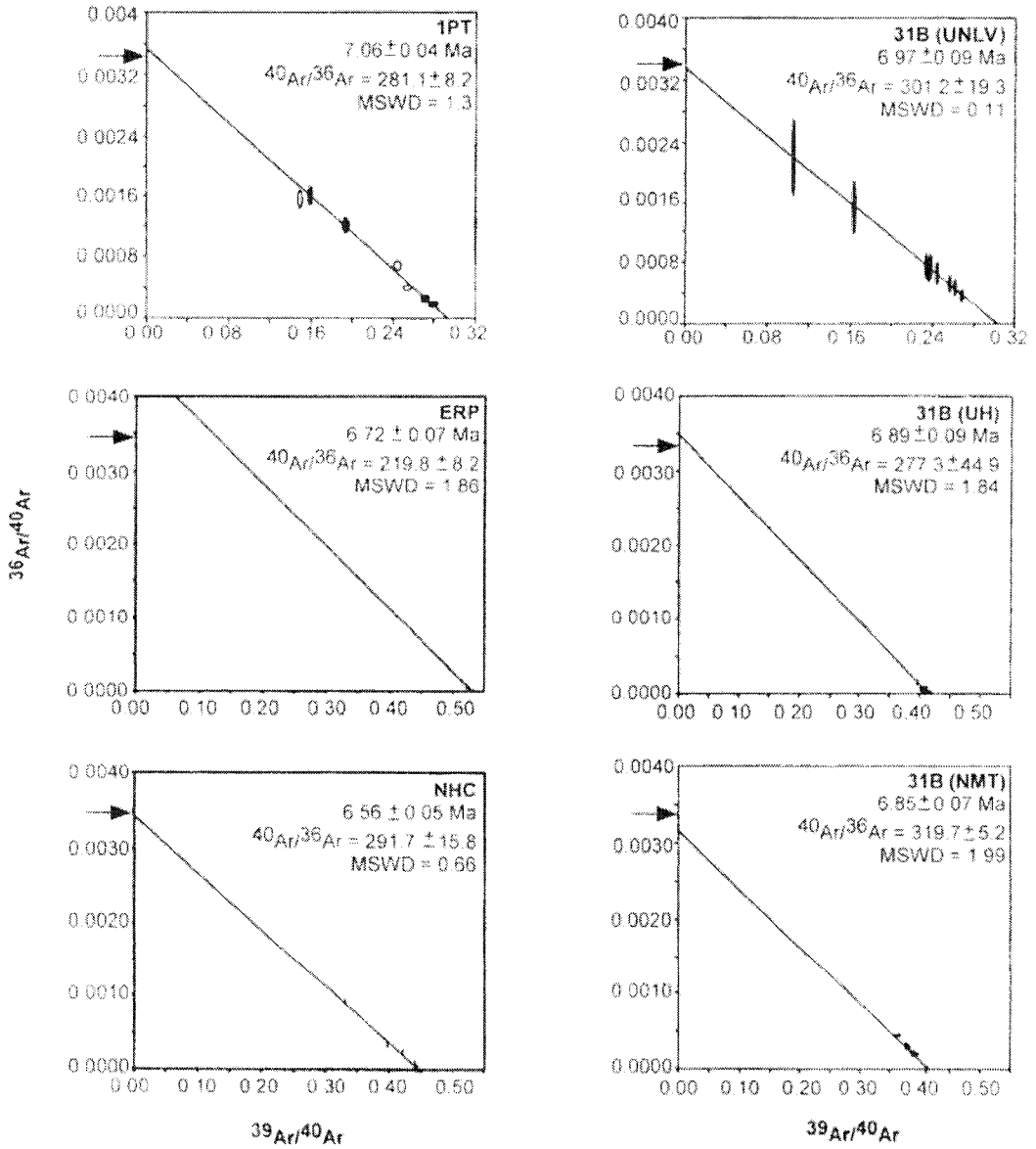

Fig. 5. Representative isochron plots for single crystal $^{40}Ar/^{39}Ar$ analyses of Bearhead Rhyolite samples. Analyses defining the isochron are shown by solid ellipses while those omitted are shown by open ellipses. Error ellipses are shown at 2σ. Arrows on the $^{36}Ar/^{40}Ar$ axis indicate the composition of atmospheric argon.

University of Nevada, Las Vegas and the University of Michigan, respectively. Major and minor element contents of melt inclusions in quartz were determined by electron and ion microprobe techniques at New Mexico Institute of Mining and Technology and Arizona State University. $^{40}Ar/^{39}Ar$ dating of single feldspar crystals was completed at the University of Houston, New Mexico Institute of Mining and Technology, and the University of Nevada, Las Vegas. Representative examples of $^{40}Ar/^{39}Ar$ dates

Table 1
Summary of $^{39}Ar/^{40}Ar$ ages of the Bearhead Rhyolite

Sample	Rock type	Location	Latitude	Longitude	Geochemical group	Age (Ma) (± 1σ[a])	Analysis type	Age calcu
PN	Rhyolite	Paseo del Norte	35°49′30″	106°28′49″	Paseo del Norte	1.47 ± 0.04	single crystal	weighted
CY	Rhyolite	Cerrito Yelo	35°40′04″	106°31′17″	Cerrito Yelo	6.04 ± 0.06	groups of crystals	isochron
CYE	Rhyolite	south of Cerrito Yelo	35°39′56″	106°31′08″	Cerrito Yelo	6.16 ± 0.03	single crystal	weighted
NHC	Rhyolite	north Hondo Canyon	35°42′17″	106°33′02″	Main Group	6.57 ± 0.05	single crystal	isochron
WBHP	Rhyolite	west Bearhead Peak	35°43′12″	106°29′22″	Main Group	6.52 ± 0.03	groups of crystals	weighted
RH	Rhyolite	Rabit Hill	35°47′12″	106°22′27″	Main Group	6.64 ± 0.07	single crystal	isochron
CB	Rhyolite	west of Cerro Belitas	35°44′05″	106°24′30″	Main Group	6.69 ± 0.03	groups of crystals	weighted
SEAP	Rhyolite	southeast Aspen Peak	35°45′08″	106°29′40″	Main Group	6.71 ± 0.27	groups of crystals	isochron
ERP	Rhyolite	east Ruiz Peak	35°43′10″	106°32′00″	Main Group	6.72 ± 0.07	single crystal	isochron
NBC	Rhyolite	north Bland Canyon	35°44′04″	106°26′35″	Main Group	6.74 ± 0.05	groups of crystals	weighted
NAP	Rhyolite	north Aspen Peak	35°45′37″	106°29′50″	Main Group	6.76 ± 0.09	groups of crystals	weighted
SM	Rhyolite	San Miguel Mountain	35°45′46″	106°23′25″	Main Group	6.80 ± 0.04	groups of crystals	weighted
TC	Rhyolite	east of Tres Cerros	35°42′10″	106°32′16″	Main Group	6.81 ± 0.03	groups of crystals	weighted
9202P	Rhyolite	east of Cerro Pelado	35°47′00″	106°34′08″	Main Group	6.82 ± 0.04	single crystal	isochron
SAC	Rhyolite	south Arrow Canyon	35°47′09″	106°21′36″	Main Group	6.82 ± 0.04	single crystal	isochron
8843P	Rhyolite	west Hondo Canyon	35°42′07″	106°33′36″	Main Group	6.87 ± 0.07	single crystal	isochron
CJ	Rhyolite	Cerro La Jara	35°42′28″	106°30′56″	Main Group	6.90 ± 0.02	single crystal	weighted
DB	Rhyolite	west Bearhead Peak	35°43′02″	106°29′22″	Main Group	6.91 ± 0.03	single crystal	weighted
CP	Rhyolite	Cerro Picacho	35°44′35″	106°22′40″	Main Group	6.92 ± 0.03	groups of crystals	weighted
HB	Rhyolite	southwest Peralta Canyon	35°41′16″	106°29′15″	Main Group	6.97 ± 0.09	groups of crystals	isochron/
WR	Rhyolite	Woodard Ridge	35°46′30″	106°30′00″	Main Group	7.01 ± 0.06	single crystal	isochron
HPT	Tuff	south Bland Canyon	35°42′04″	106°24′40″	Main Group	7.06 ± 0.04	single crystal	isochron
EBHP	Rhyolite	east Bearhead Peak	35°43′35″	106°28′21″	Main Group	7.06[b]	single crystal	weighted
GBR	Rhyolite	northwest Cerrito Yelo	35°40′40″	106°32′11″	Older Rhyolite	7.92 ± 0.32	single crystal	isochron
SHC	Rhyolite	south Hondo Canyon	35°42′00″	106°33′17″	Trachydacite	8.92 ± 0.98	single crystal	isochron
NECY	Rhyolite	northeast Cerrito Yelo	35°40′58″	106°30′36″	Trachydacite	11.09 ± 1.57	single crystal	weighted

[a] 0.5% error is included.
[b] No error reported due to small number of analyses.

Table 2
Representative analyses for geochronology of the Bearhead Rhyolite

$^{40}Ar/^{39}Ar$	$^{37}Ar/^{39}Ar$	$^{36}Ar/^{39}Ar$ ($\times 10^{-3}$)	$^{39}Ar_K$ ($\times 10^{-15}$ mol)	K/Ca	% $^{39}Ar^*$	Age (Ma)	1σ (Ma)	Laboratory
ERPL, $J = 1.614 \times 10^{-3}$, single sanidine crystals								
2.430[a]	*−0.0879*	*0.4240*	*3.15*	*5.8*	*92.3*	*6.52*	*0.06*	*NMT*
2.543	0.0106	0.7230	24.1	48.1	88.9	6.57	0.05	NMT
2.452	0.0058	0.3780	34.2	88.4	92.7	6.61	0.05	NMT
2.369	0.0047	0.0706	17.6	108.6	96.2	6.62	0.05	NMT
2.459	0.0100	0.3580	19.9	51.0	92.9	6.64	0.05	NMT
2.416	0.1861	0.2540	5.00	2.7	94.6	6.65	0.06	NMT
2.396	0.0054	0.1240	11.8	95.2	95.6	6.66	0.05	NMT
2.439	0.0088	0.2510	12.5	58.0	94.2	6.68	0.05	NMT
2.450	0.0059	0.2840	4.37	86.5	93.8	6.68	0.06	NMT
2.408	0.0021	0.1310	20.2	241.8	95.5	6.69	0.05	NMT
2.406	0.0001	0.1160	13.4	4515.1	95.7	6.69	0.05	NMT
2.407	0.0642	0.1320	16.1	7.9	95.7	6.70	0.05	NMT
2.404	0.0002	0.0688	10.4	2538.3	96.3	6.73	0.05	NMT
2.414	0.1097	0.1310	6.87	4.7	95.9	6.73	0.06	NMT
2.447	0.0875	0.1900	7.51	5.8	95.4	6.77	0.06	NMT
					Mean:	6.66	0.06	
NHC, $J = 1.624 \times 10^{-3}$, single sanidine crystals								
2.310	0.0009	0.1320	8.23	299.3	95.4	6.44	0.15	UH
2.445	0.0107	0.5640	11.7	261.5	90.4	6.46	0.11	UH
3.091	0.0125	2.7570	9.06	225.1	71.4	6.46	0.14	UH
2.345	0.0105	0.1640	9.94	183.3	95.0	6.52	0.13	UH
2.333	0.1219	0.0920	13.6	23.1	96.2	6.57	0.09	UH
2.331	0.0087	0.0500	11.8	323.9	96.4	6.57	0.11	UH
2.325	0.0094	0.0150	13.3	300.4	96.9	6.59	0.11	UH
2.348	0.0110	0.0780	19.7	256.6	86.1	6.60	0.07	UH
2.593	0.0120	0.0840	16.8	233.5	87.8	6.66	0.08	UH
					Mean:	6.54	0.08	
31B, $J = 1.590 \times 10^{-3}$, single sanidine crystals and ** = 3–9 sanidine crystals								
2.793	0.0177	1.2280	47.30	28.8	84.6	6.76**	0.05	NMT
2.591	0.1309	0.5197	16.40	3.9	91.8	6.81**	0.06	NMT
2.378	0.0123	0.2070	20.40	227.9	94.1	6.81	0.09	UH
2.615	0.0105	0.5519	33.80	48.8	91.2	6.82**	0.05	NMT
2.382	0.0444	0.3170	17.2	63.3	93.7	6.82**	0.10	UH
2.701	0.0146	0.8243	33.40	34.9	88.5	6.84**	0.06	NMT
2.398	0.0000	0.0320	17.8	–[b]	96.8	6.86	0.09	UH
2.634	0.0128	0.5667	35.40	39.8	91.1	6.87**	0.06	NMT
2.604	0.0170	0.4589	30.30	30.1	92.2	6.87**	0.06	NMT
2.401	0.0024	0.1820	30.50	1153.5	95.1	6.87	0.09	UH
2.682	0.0323	0.7077	31.2	15.8	89.2	6.89**	0.06	NMT
3.039	0.0303	1.9100	36.8	16.8	79.2	6.90**	0.06	NMT
2.411	0.0000	0.4040	18.5	–	92.7	6.90	0.09	UH
2.428	0.0041	−0.0210	16.5	683.9	97.5	6.95	0.10	UH
2.427	0.0064	0.0600	11.8	441.7	96.5	6.95	0.11	UH
2.454	0.0000	0.0100	11.7	–	97.1	7.03	0.11	UH
2.461	0.0055	−0.0650	10.1	512.1	98.0	7.04**	0.01	UH
2.469	*0.0000*	*0.0370*	*14.7*	–	*96.8*	*7.07***	*0.10*	*UH*
					Mean:	6.89	0.07	

[a] Italics denote an analysis whose age lies outside of 2σ of the mean age.
[b] – denotes infinite K/Ca.

Table 4
Representative analyses for geochronology of the Bearhead Rhyolite

^{36}Ar	^{37}Ar	^{38}Ar	^{39}Ar	^{40}Ar	$(^{40}Ar/^{39}Ar)_K$	K/Ca	$\%^{40}Ar^*$	Age (Ma)	1σ (Ma)	Laboratory
31B, $J = 1.1503 \times 10^{-3}$, single sanidine crystals										
1.41	0.472	1.139	66.829	637.853	3.4943	14.1	36.6	7.24	0.06	UNLV
0.35	0.289	1.482	110.482	473.530	3.3952	38.1	79.4	7.03	0.05	UNLV
1.08	0.316	1.707	116.237	711.670	3.4537	36.6	56.4	7.15	0.05	UNLV
0.16	0.234	1.181	87.529	336.252	3.3545	37.2	87.8	6.95	0.05	UNLV
0.15	0.144	0.609	44.587	189.899	3.3245	30.8	79.1	6.89	0.06	UNLV
0.34	0.167	0.665	49.249	204.046	3.3386	29.4	81.5	6.92	0.05	UNLV
0.16	0.314	1.577	120.751	451.634	3.3681	38.3	90.3	6.98	0.05	UNLV
0.22	0.264	1.234	89.703	380.870	3.3797	33.8	79.9	7.00	0.05	UNLV
0.22	0.300	1.467	108.867	425.930	3.3361	36.1	85.6	6.91	0.05	UNLV
							Mean:	7.01	0.12	
1PT, $J = 1.1423 \times 10^{-3}$, single sanidine and plagioclase crystals										
0.07	0.269	1.424	107.79	389.029	20.3712	41.5	95.1	7.03	0.05	UNLV
0.08	2.799	0.152	10.686	58.309	0.1918	0.4	65.2	6.95	0.09	UNLV
0.10	0.242	1.122	84.376	313.702	17.6939	36.1	92.0	6.99	0.05	UNLV
0.15	3.382	0.215	13.526	88.113	0.1190	0.4	53.4	6.96	0.06	UNLV
0.04	2.55	0.14	10.506	46.274	0.2070	0.4	81.5	6.89	0.07	UNLV
0.13	0.433	2.361	180.368	646.277	21.1909	43.2	94.3	6.95	0.05	UNLV
0.10	0.276	1.445	108.436	401.778	19.9731	40.7	92.3	7.01	0.11	UNLV
0.09[a]	*2.915*	*0.103*	*6.895*	*49.547*	*0.1189*	*0.2*	*56.3*	*7.82*	*0.08*	*UNLV*
0.12	0.302	1.451	109.857	406.858	18.4774	37.7	91.9	6.98	0.05	UNLV
0.11	0.184	0.821	61.752	246.135	17.0334	34.8	88.2	7.17	0.05	UNLV
							Mean:	6.99	0.08	

[a] Italics denote an analysis whose age lies outside of 2σ of the mean age

are shown in Figs. 4 and 5 and Table 1. Complete data sets of each analysis are available from the authors upon request. Details of analytical methods and data treatment are discussed in Appendix A.

5. Space and time trends in the Bearhead Rhyolite dome field

A total of 26 new $^{40}Ar/^{39}Ar$ dates were obtained on Bearhead Rhyolite domes (Tables 1–3). These compliment nine previously published K/Ar ages on the Bearhead Rhyolite which range from 8.7 ± 0.7 to 5.8 ± 0.2 Ma (Leudke and Smith, 1978; Gardner and Goff, 1984; Gardner et al., 1986), and overlap with the five $^{40}Ar/^{39}Ar$ ages on the Peralta Tuff which range from 6.96 ± 0.10 to 6.75 ± 0.09 Ma (McIntosh and Quade, 1995). The majority of dated samples (~82%) were erupted over an ~540 ka interval (7.06 ± 0.04–6.52 ± 0.03 Ma) and includes most of the Peralta Tuff section. As discussed below, these rocks comprise the chemically coherent Main Group (Table 1). In contrast, two trachydacite domes (SHC, 8.92 ± 0.98 Ma and NECY, 11.09 ± 1.57 Ma) were erupted ~9–11 Ma in the southwestern part of the dome field and a low-silica rhyolite (GBR, 7.92 ± 0.32 Ma) was erupted ~8 Ma along the western margin of the dome field and are, therefore, older than the Main Group of Bearhead Rhyolite samples. Additionally, one group (CY, 6.04 ± 0.06 Ma and CYF, 6.16 ± 0.03 Ma) was erupted ~6.1 Ma in the southwestern part of the dome field near Cerrito Yelo. The dome at Paseo del Norte (PN) was erupted 1.47 ± 0.04 Ma, and thus is associated with the younger Valles/Toledo calderas.

In Fig. 6 the preferred ages from Table 1 are summed to produce a single frequency distribution plot that shows patterns in the timing of Bearhead Rhyolite and Peralta Tuff eruptions. Based on eruptive frequency, the first significant phase of volcanism, lasting from 7.06 ± 0.04 Ma to 6.71 ± 0.27 Ma, may have been more active than all later phases and includes all of the Peralta Tuff dated by McIntosh and

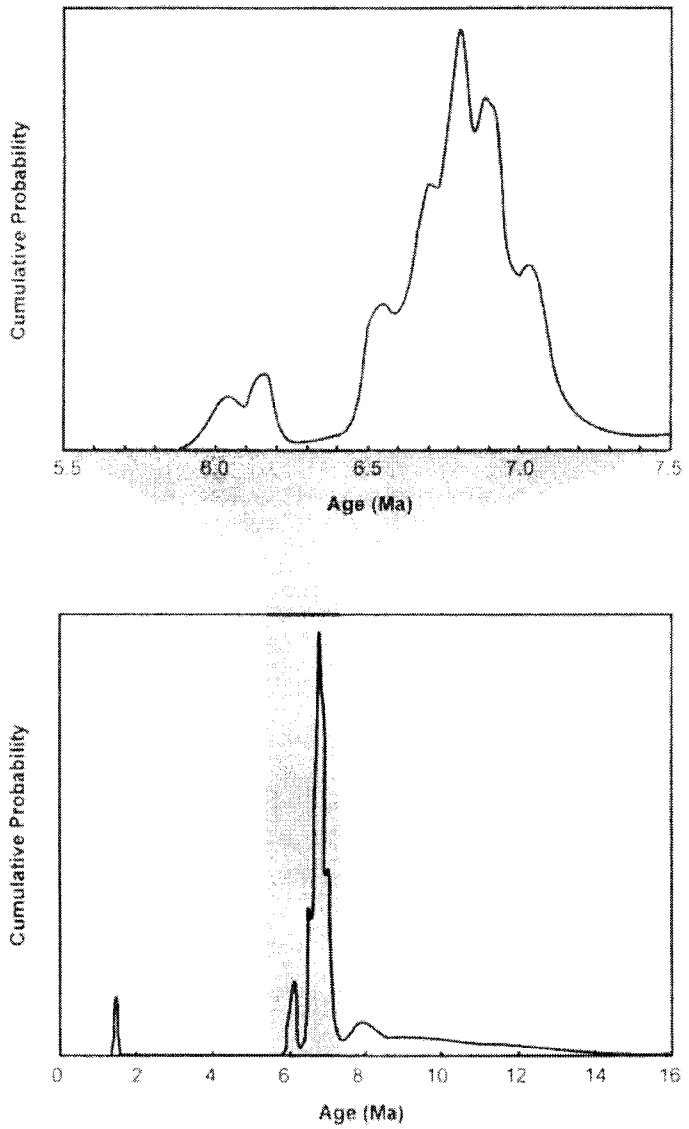

Fig. 6. Probability distribution diagram depicting the eruptive periodicity of the Beaihead Rhyolite. Sample ages and standard deviations used are preferred $^{40}Ar/^{39}Ar$ ages and their associated errors from Table 1.

Quade (1995). During this interval of time, volcanism spanned the entire dome field (an ~200 km^2 area). After this initial period, volcanic activity rapidly decreased until around 6.52 Ma when eruptive activity nearly ceased. During this ~200 ka interval of time (6.7–6.5 Ma), volcanic activity shifted northward in two 100 ka eruptive intervals. After a ~450 ka period of quiescence, a second group of rhyolite domes erupted at ~6.1 Ma in the southwestern portion of the dome field around Cerrito Yelo. It appears that volcanism in the dome field had completely ceased after ~6 Ma.

Table 4

Beartrad Rhyolite whole rock major and trace element abundances

[illegible]	[illegible]	[illegible]	[illegible]	[illegible]	[illegible]	[illegible]	[illegible]	[illegible]	[illegible]	[illegible]	[illegible]	[illegible]	[illegible]	[illegible]	[illegible]	[illegible]	[illegible]	[illegible]	[illegible]	[illegible]	[illegible]	[illegible]	[illegible]	[illegible]	[illegible]	[illegible]	[illegible]	[illegible]	[illegible]	[illegible]	[illegible]	[illegible]
[illegible]	[illegible]	[illegible]	[illegible]	[illegible]	[illegible]	[illegible]	[illegible]	[illegible]	[illegible]	[illegible]	[illegible]	[illegible]	[illegible]	[illegible]	[illegible]	[illegible]	[illegible]	[illegible]	[illegible]	[illegible]	[illegible]	[illegible]	[illegible]	[illegible]	[illegible]	[illegible]	[illegible]	[illegible]	[illegible]	[illegible]	[illegible]	[illegible]

Table 5
Peralta Tuff whole rock major and trace element abundances

wt%	CF	CAN	FF	IRD	IRC	IRB	IRA	SP	CC5	CC1	FC2	FB	FC1	ZP1	FX	DH1	FT2	FWM2	AWM1	TG
SiO_2	73.9	75.2	74.4	69.3	75.6	76.6	75.8	76.9	74.4	74.7	71.9	74.8	75.5	69.5	71.1	75.6	74.4	75.2	75.4	74.4
Al_2O_3	12.6	11.8	11.8	11.5	12.5	12.7	12.5	11.3	12.1	12.5	12.0	11.8	11.4	12.6	12.5	12.6	11.7	12.1	12.4	12.3
TiO_2	0.1	0.1	0.1	0.1	0.1	0.1	0.1	0.1	0.1	0.1	0.1	0.1	0.1	0.1	0.1	0.1	0.1	0.1	0.1	0.1
$Fe_2O_3^T$	0.6	0.5	0.5	0.8	0.6	0.5	0.5	0.5	0.6	0.5	0.8	0.5	0.6	0.5	0.5	0.6	0.8	0.6	0.8	0.6
MgO	<0.1	<0.1	<0.1	<0.1	0.1	0.1	<0.1	0.1	<0.1	0.1	<0.1	0.1	0.2	0.4	0.5	0.1	<0.1	<0.1	0.1	0.1
CaO	0.4	<0.3	0.3	<0.3	<0.3	<0.3	<0.3	<0.3	<0.3	<0.3	0.4	<0.3	0.4	<0.3	<0.3	<0.3	<0.3	<0.3	<0.3	<0.3
Na_2O	2.6	3.0	2.9	3.4	3.5	3.1	2.8	3.9	3.4	2.9	3.4	2.8	2.9	2.5	3.1	2.6	2.3	3.1	2.7	3.1
K_2O	5.5	5.1	4.6	4.8	4.0	4.9	5.2	5.3	4.5	5.1	4.0	5.0	5.1	5.0	5.2	5.5	5.4	5.0	5.4	4.9
MnO	0.049	0.061	0.038	0.066	0.065	0.063	0.016	0.064	0.061	0.038	0.066	0.065	0.063	0.019	0.017	0.058	0.068	0.078	0.010	0.049
P_2O_5	<0.04	<0.04	0.06	<0.04	0.04	<0.04	0.06	<0.04	<0.04	<0.04	0.06	0.07	0.05	<0.04	0.07	<0.04	0.04	<0.04	0.07	<0.04
LOI	4.85	4.05	3.65	4.71	3.43	3.05	5.19	5.50	5.17	5.43	4.81	4.74	4.26	5.16	4.59	5.22	5.16	5.12	4.52	4.65
Total	100.6	99.9	98.1	94.0	100.6	103.4	99.6	101.8	100.4	101.6	97.4	100.0	102.5	98.7	101.7	100.4	100.4	100.7	99.3	94.0
ppm[a]																				
Rb*	150	132	129	119	119	124	134	136	118	122	126	139	109	150	126	115	123	132	119	116
Sr*	46	17	28	40	30	<3	<7	31	21	30	17	25	59	54	24	32	22	24	22	27
Y*	6	22	15	19	24	21	18	14	30	18	30	14	24	24	29	24	16	19	23	21
Zr*	70	93	70	76	74	75	80	67	92	77	89	82	81	75	82	73	67	78	82	78
Nb*	23	34	14	22	26	26	22	17	37	16	37	20	23	23	35	30	14	18	25	23
Ba**	88	666	526	662	678	646	775	623	637	577	564	558	669	172	472	535	580	567	414	677
Sc**	1.9	2.9	2.7	2.0	2.9	2.9	2.9	2.8	3.1	3.2	3.2	3.2	3.1	3.8	3.7	3.1	3.3	3.2	3.4	3.2
Ce**	15	18	16	15	19	21	25	23	26	26	24	29	25	13	23	41	38	40	26	28
Cs**	0.5	4.9	4.5	4.2	4.1	4.2	4.4	4.6	3.9	4.4	4.5	5.5	3.9	3.3	4.2	6.1	4.7	4.2	4.5	4.2
Eu**	29	26	24	27	<0.75	26	27	23	28	27	28	<0.77	23	46	26	37	24	24	24	38
Gd**	46	49	48	51	52	51	51	48	56	56	57	49	46	37	54	52	51	46	49	54
Nd**	<26	<26	<26	7	<26	21	<23	<21	<22	27	<26	16	12	7	16	27	12	18	18	26
Sm**	1.5	3.7	3.5	4.1	4.0	3.9	3.9	3.6	4.3	4.1	4.2	4.1	3.9	3.6	4.2	4.3	4.3	4.1	4.3	4.1
Eu**	0.2	0.4	0.4	0.4	0.5	0.5	0.5	0.5	0.5	0.5	0.6	2.6	0.5	0.4	0.5	0.5	0.5	0.5	0.5	0.5
Tb**	0.2	0.6	0.5	0.5	0.5	0.6	0.6	0.5	0.7	0.6	0.6	0.7	0.7	0.6	0.6	0.6	0.7	0.6	0.7	0.6
Yb**	3.4	2.1	2.6	2.4	2.4	2.3	2.6	2.1	2.5	2.3	2.5	2.6	2.5	3.0	2.6	2.3	3.1	2.6	2.5	2.6
Lu**	0.3	0.3	0.2	0.3	0.3	0.4	0.3	0.4	0.4	0.3	0.4	0.4	0.3	0.3	0.4	0.4	0.4	0.3	0.4	0.3
Hf**	3.4	3.5	3.4	3.5	3.7	3.4	3.7	3.3	3.9	3.9	4.0	3.6	3.8	3.0	3.9	3.7	3.9	3.7	4.0	3.8
Ta**	2.2	2.3	2.3	2.7	2.8	2.6	2.5	2.5	2.1	2.3	2.2	2.6	3.0	3.0	2.9	2.5	2.8	2.1	2.6	2.1
Th**	20.9	12.2	11.9	13.3	11.9	11.6	11.8	10.7	11.9	11.6	11.9	11.3	10.8	11.5	11.8	11.2	11.7	11.3	11.7	11.2
U*	8.5	4.4	5.0	4.0	4.5	3.4	4.8	4.7	4.6	4.4	3.4	4.5	3.8	4.1	3.7	5.7	4.5	5.0	4.7	4.0

[a] Total Fe expressed as Fe_2O_3.
[b] *XRF; **INAA.

6. Petrography

Bearhead Rhyolite samples are massive to continuously flow banded, and include vitrophyre and pumiceous rhyolite. The groundmass in most rhyolite samples is devitrified. The Peralta Tuff is composed of primary, distal and reworked pyroclastic fall deposits, pyroclastic flow deposits, and surge deposits. Most Bearhead Rhyolite units are nearly aphyric to sparsely porphyritic, containing an average of 4 ± 3% phenocrysts (Justet, 1999). Samples SH1 and SH2 are aphyric whereas phenocryst-rich domes and flows in the far northwest and southwest of the dome field (CY, CYF, NECY, PN, and NHC) contain a significantly higher average of 21 ± 4% phenocrysts. These petrographically distinct samples are also chemically distinct from the Main Group, as discussed below.

Phenocryst phases consist of quartz, sanidine, plagioclase, biotite, zircon, allanite, and apatite, in decreasing order of abundance. Quartz, sanidine, and plagioclase occur together as individual phenocrysts, phenocryst fragments, and poly- and monomineralic glomerocrysts. Most samples have average modal abundances of 35% quartz, 60% sanidine, 1% plagioclase. These felsic phases comprise 81–100% of phenocryst assemblages (Justet, 1999). The relative amounts of quartz, sanidine, and plagioclase vary little from sample to sample except for samples NECY in which plagioclase is the dominant phase and PN in which quartz is the dominant phase. Most felsic phenocrysts range from <100 μm to 2.5 mm and within a single thin section are euhedral to anhedral, and are commonly embayed. Sanidine may be untwinned, or show carlsbad twins, baveno twins, oscillatory zoning along phenocryst rims, and continuous zoning from core to rim. Less commonly, plagioclase is moderately embayed, and exhibits polysynthetic twins, carlsbad twins, discontinuous, and oscillatory zoning. Highly embayed quartz is common, especially in fractured phenocrysts where embayments appear to follow cracks.

Biotite and magnetite are the only significant mafic phases present in all Bearhead Rhyolite samples. The typical ratio of mafic to felsic phenocrysts is 1:20. Most samples contain ≤1% of biotite, but samples NECY and SHC contain an average of 2% biotite (Justet, 1999). Biotite phenocrysts and crystal fragments are generally euhedral and unaltered. Magnetite forms ≤1% of the modal phenocryst assemblage and is anhedral. Magnetite commonly overgrows small portions of glomerocrysts and biotite and appears by itself in the matrix.

The accessory mineral assemblage is composed of ~0.01% allanite, ~0.01% zircon, and ~0.01% apatite and were observed in several Bearhead Rhyolite and Peralta Tuff samples. Allanite phenocrysts are typically <200 μm in diameter, equant, and euhedral. Allanite occurs as separate phenocrysts in the matrix as well as within glomerocrystic sanidine, biotite, and magnetite. Zircon phenocrysts are commonly equant, euhedral, and unresorbed (Justet, 1999) and occur as separate phenocrysts in the matrix and in clusters associated with biotite, opaque oxides, and, less commonly, feldspars. Zircon crystals range from 300 to 400 μm in diameter. Apatite was observed in a few samples as 10–15 μm long needles.

7. Geochemistry of the Bearhead Rhyolite and Peralta Tuff

Most analyzed samples are high-silica rhyolite (SiO_2 > 75 wt%) using the Le Bas et al. (1986) classification and have very similar major element compositions (Tables 4 and 5). Two samples classify as trachydacites (SHC and NECY) and one sample is a low-silica rhyolite (GBR), all of which are located on the southwestern periphery of the dome field north of Cerrito Yelo and are significantly older than the Main Group (Fig. 2, Table 1). The trace element data and rare earth elements (REEs), suggest two distinct geochemical groups exist within the high-silica rhyolite samples in addition to the trachydacite and low-silica rhyolite samples discussed above (Figs. 7 and 8). Samples can thus be divided into distinct geochemical groups as follows: (1) trachydacite domes SHC and NECY; (2) low-silica rhyolite dome GBR and high-silica rhyolite dome at Spring Hill (SH1 and SH2); (3) high-silica rhyolite dome Cerrito Yelo (CY and CYF) and Cochiti Formation sample CF; and (4) all other high-silica Bearhead Rhyolite domes and flows and all Peralta Tuff, referred to as the Main Group.

7.1. Trachydacite domes

The trachydacite domes (SHC and NECY) are

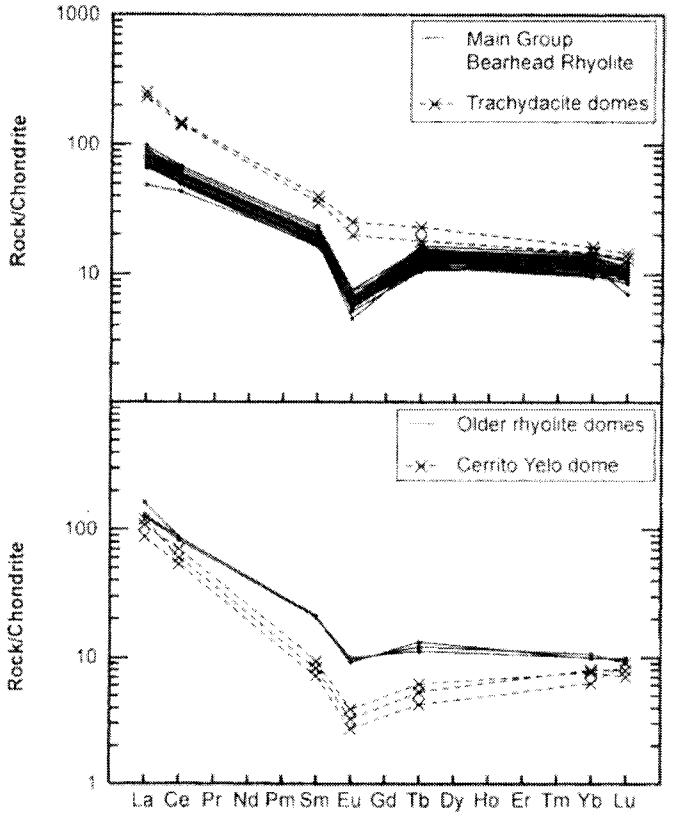

Fig. 7. REE/Chondrite plots for the Bearhead Rhyolite, Tracydacite domes, SHC, NECY; older rhyolite domes, GBR, SH1, SH2, and Cerrito Yelo domes, CY, CYF, CF. Chondrite values are from Nakamura (1974).

distinguished from all other Bearhead Rhyolite samples by their significantly older ~9–11 Ma eruptive age (Table 1), petrography, major and trace element composition, elevated LREE concentrations compared to other samples', poorly developed negative Eu anomaly (Eu/Eu* = 0.9) (Fig. 7), and location in the southwestern periphery of the dome field (Fig. 2). For example, the trachydacite samples contain 20–27% phenocrysts compared to the Main Group which contains <6% phenocrysts. In trace element chemistry, the trachydacite domes are distinguished from all other samples by their elevated Zr, Th (Fig. 8), and Hf abundances.

7.2. Older rhyolite domes

The low-silica rhyolite dome (GBR) and high-silica rhyolite dome at Spring Hill (SH1 and SH2) are distinguished from all other Bearhead Rhyolite samples by the older 7.92 Ma eruptive age for GBR (Table 1), distinctive REE patterns, major and trace element geochemistry (Fig. 8), poorly developed Eu anomaly (Eu/Eu* = 0.6) (Figs. 7 and 8), and location in the western periphery of the dome field (Fig. 2). Petrographically, these domes are similar to the Main Group.

7.3. Cerrito Yelo

Cerrito Yelo dome samples (CY and CYF) and the sample from Cochiti Formation volcaniclastic sediment (CF) (Fig. 3) are characterized by their distinctly younger ~6.1 Ma eruptive age (Table 1), petrography, distinct trace element geochemistry (Fig. 8),

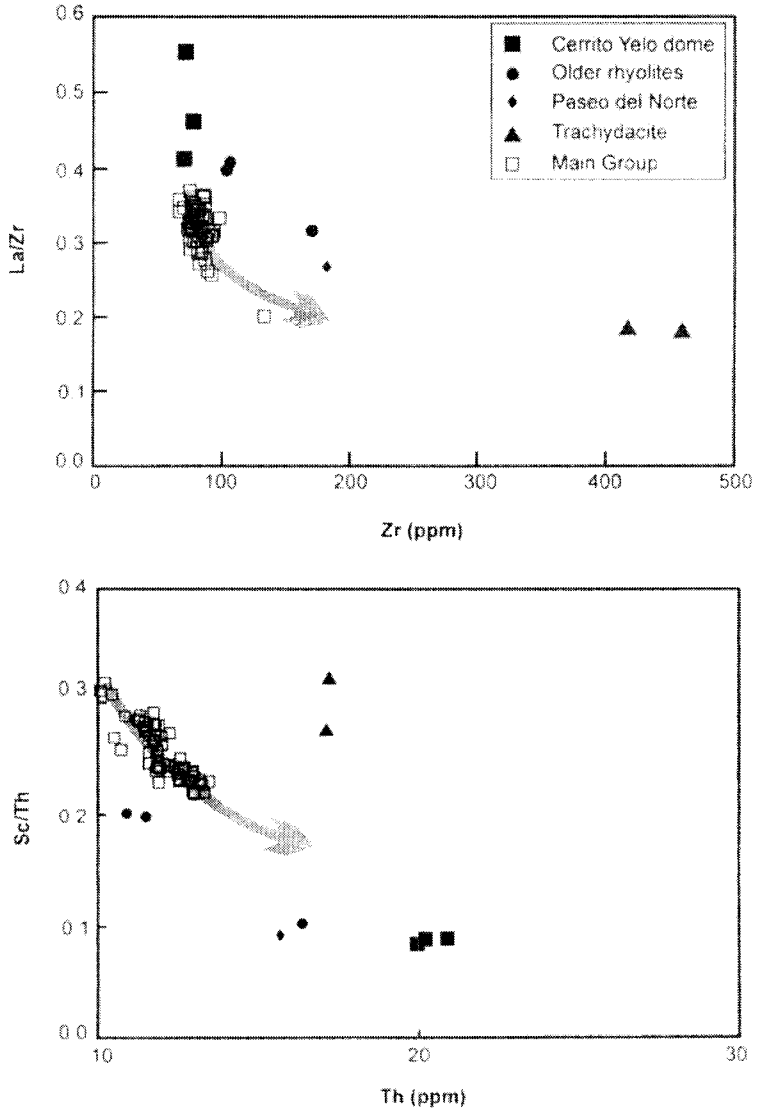

Fig. 8. Trace element ratio plots of the Bearhead Rhyolite depicting the chemical coherency of the Main Group. Analytical uncertainty is smaller than the symbols. Gray arrows indicate hypothetical Rayleigh fractionation trends by removal of the modal mineral assemblage observed for Main Group samples.

poorly developed Eu anomaly (Eu/Eu* = 0.5) and steep LREE trends (Fig. 7), and their location in the southwestern periphery of the dome field (Fig. 2). Each sample contains 16–20% phenocrysts compared to the Main Group which contains <6% phenocrysts. In trace element chemistry, the Cerrito Yelo and Cochiti Formation samples are distinguished by their low Zr, and high Th and Hf abundances (Fig. 8). The chemical and petrographic similarity between Cerrito Yelo dome samples and the Cochiti Formation sample, the younger ages of the dome samples and the younger relative age (e.g. higher

Table 6
F and H_2O contents of melt inclusions from Peralta Tuff quartz

Sample[a]	F (wt%)	H_2O (wt%)	Sample[a]	F (wt%)	H_2O (wt%)
TWM1			TA		
1/1	0.00		1/1	0.05	
1/3	0.05		1/2	0.00	3.21
2/1	0.05	3.53	1/3	0.30	
2/2	0.05	3.45	1/4	0.00	
2/3	0.35		1/5	0.01	
2/4	0.14		2/1	0.19	
3/1	0.00		2/2	0.11	
3/2	0.02		2/3	0.01	
3/3	0.00		CAN		
3/4	0.00		1/1	0.07	
3/5	0.05		1/2	0.01	
4/1	0.00	2.20	1/4	0.00	
4/2	0.00		1/5	0.00	
4/3	0.19	1.75	1/6		
4/4	0.11		2/1	0.00	4.33
4/5	0.07		2/2	0.00	
4/6	0.07	2.73	2/3	0.00	4.11
4/7	0.00	2.31	2/4	0.00	
CC3			2/5	0.06	2.25
2/1	0.12	2.88	3/1	0.06	
2/2	0.02	2.55	3/2	0.38	
2/3	0.01	3.42	3/3	0.07	3.96
3/1	0.00	2.85	3/4	0.00	
3/2	0.06	3.32	3/5	0.06	
4/1	0.21		3/6	0.16	3.68
4/2	0.25		3/7	0.05	
			4/1	0.21	2.63

[a] phenocryst#/analysis#.

stratigraphic position relative to the Peralta Tuff) of the Cochiti Formation sample suggests that sample CF represents a pyroclastic phase of the eruption which produced Cerrito Yelo (Fig. 3).

7.4. Main Group high-silica rhyolite

The majority (~82%) of analyzed Bearhead Rhyolite and all Peralta Tuff samples are remarkably similar in their major and trace element compositions (e.g. low Th and Hf) (Fig. 8) and petrography. These samples define a coherent group on REE plots (Fig. 7). Elements which are typically strongly compatible or incompatible in rhyolitic systems such as La, Ce, Zr, Hf, and Th do not vary significantly, whereas other trace elements such as Y, Yb, Sr, Ta, Tb, Lu, Nd, Cs, and U may vary by up to 2–3 fold (Tables 4 and 5).

7.5. Microprobe analysis of Main Group samples

Electron microprobe traverses across two sanidine phenocrysts from Peralta Tuff samples TWM1 and 2 reveal no significant compositional variation from $Or_{59}Ab_{40}An_1$. An additional electron microprobe traverse across a sanidine phenocryst from Peralta Tuff sample CC3 reveals an initial increase in Na_2O and decrease in K_2O from core to rim ($Or_{67}Ab_{31}An_1$–$Or_{56}Ab_{43}An_1$) followed by a composition similar to samples TWM1 and 2.

Ion microprobe analyses of glass inclusions from four quartz phenocrysts from Peralta Tuff samples reveal that Main Group magma contained an average of 3.3 wt% H_2O (Table 6). The stratigraphically lowest sample in the Peralta Tuff section has a higher water content than the other samples (~4.3 wt% H_2O) while the remainder of the section

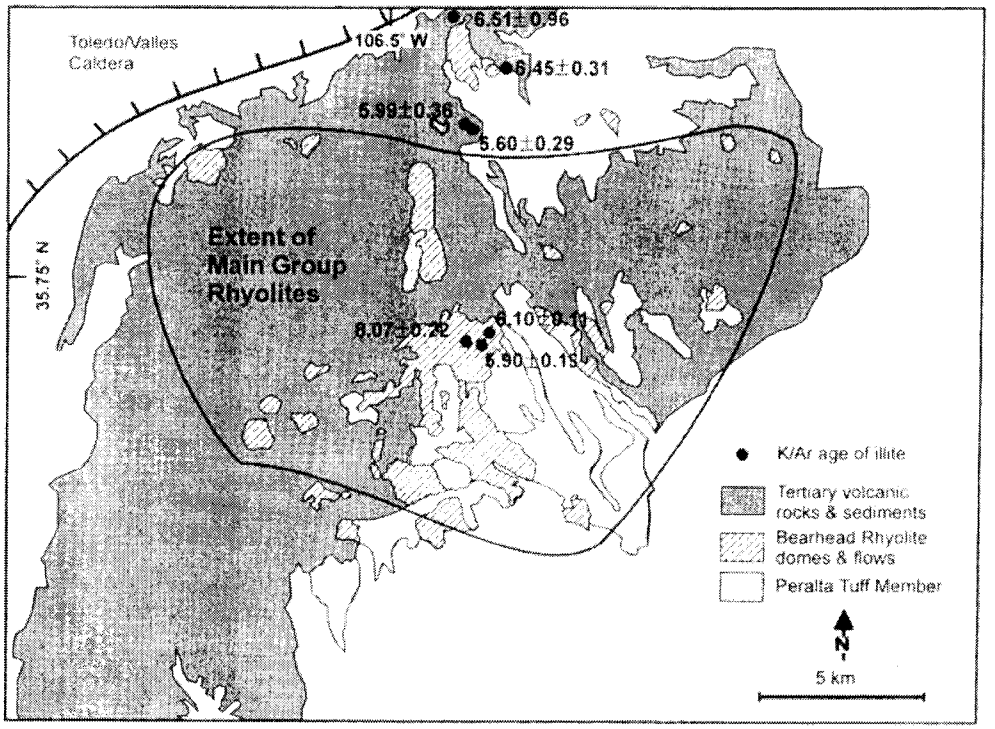

Fig. 9. Map of the Bearhead Rhyolite dome field depicting the space and time relationship between a hydrothermal event reported by WoldeGabriel and Goff (1989) and eruption of the Bearhead Rhyolite. Map after Smith et al. (1970).

displays little variation in water content from the mean.

8. Discussion

8.1. Petrogenesis of Main Group samples

The chemical coherency of the Main Group and differences compared to other groups (Figs. 7 and 8) suggest that it was derived from a single, distinct parental magma. Fractional crystallization (FXL) or assimilation-fractional crystallization (AFC) trends calculated using the observed phenocryst assemblages reproduce trends in Main Group chemistry. However, FXL and AFC trends in the Main Group do not reproduce compositions of the Cerrito Yelo, low-silica rhyolite, or trachydacite groups (Fig. 8). These relationships suggest that the other geochemical groups cannot be related to the Main Group by processes likely to occur at shallow crustal levels such as FXL or AFC. Ellisor (1995) reported isotopic data for Main Group samples ($^{87}Sr/^{86}Sr$, 0.7075–0.7093) that trend towards radiogenic upper crustal $^{87}Sr/^{86}Sr$ compositions at constant $^{143}Nd/^{144}Nd$ values. This trend suggests that the Sr isotopic composition of the Main Group reflects late-stage upper crustal assimilation. Thus, changes in the trace element composition of the Main Group can be explained by fractional crystallization of a parental magma with a small amount of upper crystal assimilation affecting its Sr isotopic composition due to relatively low Sr abundances in Bearhead Rhyolite magmas (Tables 4 and 5).

The high degree of chemical coherency of the Main Group and the ability of a FXL or AFC model to relate Main Group samples to each other suggests these rhyolites were derived from a single magma chamber. Distribution of Main Group domes over a ~10 by ~20 km area (Fig. 2) suggests that the magma

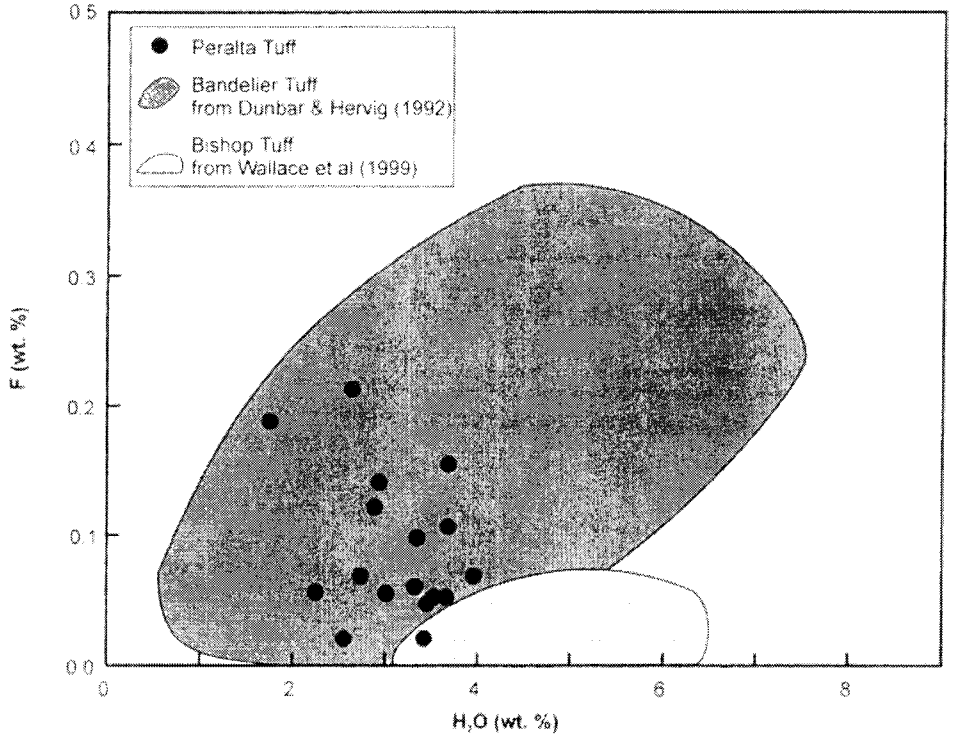

Fig. 10. H_2O versus F plot for melt inclusions in Peralta Tuff quartz and the caldera-forming eruptions of the Bandelier and Bishop Tuffs.

chamber from which the rhyolite was derived was of substantial size. The $^{40}Ar/^{39}Ar$ geochronology constrains eruption of the Main Group to an ~540 ka interval, a substantial interval for crustal magma chambers. Cooling due to conduction of heat to cold country rock as well as convective heat loss from overlying hydrothermal systems would result in crystallization of silicic magma chambers as large as 10 km diameter in <100 ka (e.g. Hawkesworth et al., 2000). Thus, this long eruptive interval requires an additional heat source such as basaltic magma to sustain the Main Group magma chamber. However, direct evidence of such a heat source (e.g. reverse-zoned phenocrysts, mafic enclaves) was not observed.

Hydrothermal alteration of rocks of the Cochiti Mining District in the center of the Bearhead Rhyolite dome field (Fig. 2) is consistent with the existence of a large shallow magma chamber during eruption of the Main Group (Fig. 9). WoldeGabriel and Goff (1989) obtained K/Ar dates on illite which ranged from ~8.1 to 5.6 Ma, with most dates in the range of ~6.5–5.9 Ma, coeval with the waning stages of Bearhead Rhyolite eruptions. The large areal distribution of this hydrothermal event (Fig. 9) is consistent with the presence of a large magma reservoir. Thus, the Main Group Bearhead Rhyolite magma chamber may have been similar in size to the shorter-lived (~390 ka) large-volume rhyolitic magma chamber(s) that produced caldera-forming eruptions of the Bandelier Tuff later in the Jemez volcanic field's history.

8.2. Effusive eruption of Main Group magmas

Factors which could control effusive versus explosive eruption of silicic magmas include: volatile content of the magma; decompression/ascent rate of the magma (Sparks et al., 1994; Barclay et al., 1996); or structural venting of a magma chamber by faults. Ion microprobe data (Table 6) suggest that the volatile content of the Peralta Tuff was comparable to that of large-volume ignimbrites such as the Bandelier Tuff and

Bishop Tuff (Dunbar and Hervig, 1992; Wallace et al., 1999) suggesting that Bearhead magma was not volatile poor (Fig. 10). The role that decompression/ascent rate may have played in controlling the volatile content of the Main Group is difficult to evaluate. However, the fact that the dome field overlies two fault zones (Cañada de Cochiti and Pajarito) that were active around the time that the Bearhead Rhyolite was erupted (Manley, 1976, 1979; Golombek, 1981, 1983; Golombek et al., 1983; Gardner, 1985) makes it likely that faulting did play a role in the effusive eruption and spatial distribution of Bearhead Rhyolite volcanism.

There are two examples of large silicic magma chambers that have yielded dominantly effusive eruptions and have not produced caldera-forming eruptions: the rhyolites of the Coso volcanic field, and the Taylor Creek Rhyolite. The main eruptive phase of the high-silica rhyolite of Coso consists of 32 chemically related domes covering ~150 km^2 that were erupted over an ~240 ka interval (Bacon et al., 1981) southeast of the Sierra Nevada Mountains. It is estimated that the total volume of the dome and flow units is ~1.6 km^3 while only ~0.3 km^3 of pyroclastic material was erupted. Detailed structural studies of the area allowed Bacon et al. (1981) to relate the effusive eruption of the Coso rhyolites to west-northwest directed Cenozoic extension and faulting in the area.

The Taylor Creek Rhyolite, in New Mexico, consists of 20 high-silica rhyolite domes and associated pyroclastic rocks that were erupted over ~800 km^2 in < 100 ka and were interpreted as being derived from a single shallow magma chamber. It is conservatively estimated that the total volume of the dome and flow units is ~55 km^3 while ~45 km^3 of pyroclastic material was erupted (Duffield and Dalrymple, 1990). It is less clear why the Taylor Creek Rhyolite magma chamber did not produce a caldera-forming eruption but has been attributed to either volatile poor magma (Duffield and du Bray, 1990; Webster and Duffield, 1991) or structural venting of magma (Duffield and Dalrymple, 1990; Duffield and Ruiz, 1992).

8.3. Influence of faulting on Main Group eruptions

Previous workers have suggested that fault activity bounding the western margin of the Española Basin shifted from the Cañada de Cochiti fault zone to the Pajarito fault zone between 5 and 6 Ma (Manley, 1976, 1979; Golombek, 1981, 1983; Golombek et al., 1983). The NE trending distribution of similarly aged, cogenetic Main Group domes (at > ~6.8 and ~6.6 Ma) suggests that the Pajarito fault zone may have been active earlier than 6 Ma. Alternatively, rhyolite domes erupted ~6 Ma are cut by the Cañada de Cochiti fault zone suggesting that the fault zone was active after 6 Ma (Gardner, 1985). The shifts in volcanism between the western to the eastern portion of the field area may suggest that both fault zones were interacting with each other at various times rather than faulting simply shifting west to east with time.

8.4. Main Group's lack of geochemical trend with time

Cogenetic suites of volcanic rocks typically exhibit progressive changes in chemistry with time or stratigraphic position. These are often interpreted as recording the progressive effects of differentiation processes such as fractional crystallization in the subvolcanic magma chamber. Despite the chemical coherency and apparent FXL/AFC trends in the Main Group, there is a lack of distinct chemical trend with increasing stratigraphic position within the Peralta Tuff or Main Group samples with time. Several possible explanations for this are discussed below.

Main Group magma may have occupied several cupolas in a single magma chamber, with magma in each cupola being isolated and evolving independently. Eruptions from independent cupolas would thus produce no chemical progression with time although they all share a common parental melt. This model is plausible because much of the Main Group occupies the highly faulted Bearhead Basin. The magma chamber may have had an irregular shape caused by upwelling of magma along faults and particularly where faults intersect.

Alternatively, the Main Group magma chamber may have been zoned with disruption of zonation occurring as the chamber was tapped or as new magma was injected from below. Subsequent sampling of the magma chamber by eruptions could produce cogenetic rhyolites lacking time or stratigraphic geochemical trends. The only possible evidence for replenishment of the Bearhead Rhyolite

magma chamber (e.g. reversed-zoned phenocrysts, resorbed phenocrysts, mafic enclaves, mafic composition phenocrysts) is the presence of resorbed phenocrysts, but decompression of the magma can achieve the same result.

A final possibility is that each Main Group eruption was derived from separate magma chambers representing separate melting events in the lower crust. However, the chemical coherency of Main Group magmas argues against this model. It seems unlikely that the Main Group was derived from a series of separate, though chemically similar lower crustal sources in light of isotopic data that suggest that the lower crust is highly heterogeneous (Reid et al., 1989; Chen and Arculus, 1989; Rudnick and Fountain, 1995).

9. Conclusions

$^{40}Ar/^{39}Ar$ age data suggest that minor amounts of chemically distinct trachydacitic, low-silica rhyolite, and high-silica Bearhead Rhyolite was erupted ~2–4 my and ~900 ka, respectively, before the majority of the Bearhead Rhyolite and Peralta Tuff (Main Group) eruptions occurred. The chemically coherent Main Group was erupted during a ~540 ka period from ~7.06 to 6.52 Ma over an area similar in size to the younger Toledo/Valles caldera. Finally, after an ~420 ka hiatus, minor amounts of genetically distinct Bearhead Rhyolite were erupted in the Cerrito Yelo area.

The chemical coherency, spatial distribution (~200 km^2), and presence of a major hydrothermal system (WoldeGabriel and Goff, 1989) during the time of Main Group eruptions support the hypothesis that these rhyolites were derived from a single, large, shallow magma chamber. The ~540 ka eruptive interval demands input of heat into the system to maintain the Bearhead Rhyolite magma chamber. This could have been provided by replenishment of the magma chamber with silicic melts, or basaltic underplating.

The volatile content of the Bearhead Rhyolite was comparable to, although slightly lower than, the Bandelier and Bishop Tuffs, two well-known caldera-forming eruptions. Thus, it is not likely that the dominantly effusive nature of Bearhead Rhyolite eruptions are the result of a volatile poor magma. The observation that Bearhead Rhyolite domes tend to occur at the intersection of faults and are sometimes themselves cut by faults suggests that the magma reservoir was intermittently vented by faulting which prevented volatiles from accumulating to levels high enough to trigger a caldera-forming eruption.

The Bearhead Rhyolite and Peralta Tuff represent a style of silicic volcanism that may be more common than realized because dome fields are not obviously related to a single event/magma chamber as are calderas and ash flow tuffs. Recognition and study of this eruptive style may lend new insight into understanding the genesis, evolution, and eruption of large volumes of silicic magma. The Bearhead Rhyolite represents a style of rhyolitic volcanism early in the history of the Jemez volcanic field which differs from the later caldera-forming eruptions of the Bandelier Tuff and thus may also have important implications for the long-term evolution of large silicic systems.

Acknowledgements

This study was funded by the Barrick Fellowship, EPSCoR/WISE Scholarship, and Bernada E. French Scholarship. The DoE Reactor Sharing Program at the University of Michigan provided INAA. W. Duffield provided helpful comments on the manuscript during review. We thank P. Copeland for access to the argon laboratory at the University of Houston, W. McIntosh for analyzing samples at the New Mexico Geochronology Research Laboratory at New Mexico Institute of Mining and Technology, N. Dunbar for electron microprobe analyses at the New Mexico Institute of Mining and Technology as well as ion microprobe work at Arizona State University. Thanks also to G. Smith for helping to obtain Peralta Tuff samples and helpful comments on the work as it progressed and Francesca Cinacola for mineral separation. Establishment of the Nevada Isotope Geochronology Laboratory at the University of Nevada, Las Vegas was funded by National Science Foundation grant EPS-9720162 to T. Spell.

Appendix A

A.1. XRF and INAA

Bearhead Rhyolite and Peralta Tuff samples were

Table 7
Comparison of $^{40}Ar/^{39}Ar$ ages (Ma ± 1σ) for intercalibration sample 3JB from the University of Houston, New Mexico Institute of Mining and Technology, and the University of Nevada, Las Vegas. (Ages at each laboratory overlap at 1σ)

NMT	UH	UNLV
6.76 ± 0.05	6.81 ± 0.09	6.89 ± 0.06
6.81 ± 0.06	6.82 ± 0.10	6.91 ± 0.05
6.82 ± 0.05	6.86 ± 0.09	6.92 ± 0.05
6.84 ± 0.06	6.87 ± 0.09	6.95 ± 0.05
6.87 ± 0.06	6.90 ± 0.09	6.98 ± 0.05
6.87 ± 0.06	6.95 ± 0.10	7.00 ± 0.05
6.89 ± 0.06	6.95 ± 0.11	7.03 ± 0.05
6.90 ± 0.06	7.03 ± 0.11	7.15 ± 0.05
Mean: 6.85 ± 0.05	7.04 ± 0.01	Mean: 6.98 ± 0.08
Isochron: 6.85 ± 0.07	7.07 ± 0.10	Isochron: 6.97 ± 0.09
	Mean: 6.93 ± 0.09	
	Isochron: 6.89 ± 0.09	

analyzed for major, minor, and selected trace elements (Rb, Sr, Nb, Y, Zr) by X-ray fluorescence techniques at the University of Nevada, Las Vegas, using procedures outlined by Norrish and Hutton (1969); Norrish and Chappell (1977). Calibration standardization was achieved using NIST 688 and MAG-1 standards. Trace elements Ba, Sc, Zn, Cs, La, Ce, Nd, Sm, Eu, Tb, Yb, Lu, Hf, Ta, Th, and U were analyzed at the University of Michigan using Instrumental Neutron Activation Analysis methods described by Jacobs et al. (1977) and Lindstrom and Korotev (1982). Calibration standardization was achieved using NIST SRM 1633a (Coal Fly Ash).

A.2. Ion/electron microprobe

Major and minor element analyses were determined on melt inclusion in quartz as well as along traverses in feldspar from six Peralta Tuff samples using electron microprobe (New Mexico Bureau of Mines and Mineral Resources) and ion microprobe (Arizona State University) procedures outlined by Hervig and Dunbar (1992). Electron microprobe analyses were standardized using NIST 610 and interlaboratory standards VG 586 (rhyolite), KE 12 (glass), orthoclase, and albite. Ion microprobe analyses used the NBS standard.

A.3. $^{40}Ar/^{39}Ar$ dating

$^{40}Ar/^{39}Ar$ dating was completed at the University of Houston (UH), New Mexico Institute of Mining and Technology (NMT), and the University of Nevada, Las Vegas (UNLV). Single feldspar crystals were fused using CO_2 lasers and delivered to MAP 215-50 mass spectrometers in ultrahigh vacuum extraction lines at each laboratory. Peak intensities were measured by electron multipliers through seven counting cycles; initial peak heights were determined by linear regression of the time of gas admission. Mass spectrometer discrimination and sensitivity were monitored by repeat analyses of atmospheric argon aliquots from an on-line pipette system. Discrimination corrections of 0.99684–1.00009 for the Houston samples (1 AMU), 1.00171–1.00080 for the New Mexico samples (1 AMU), and 1.01691–1.0213 for the Nevada samples (4 AMU) were applied to measured isotopic ratios. Estimated mass spectrometer sensitivities were $\approx 5.1 \times 10^{-17}$ mol/mV at a gain ~100 over the Faraday cup at Houston, $\approx 3.0 \times 10^{-17}$ mol/mV at a gain ~75 over the Faraday cup at New Mexico, and $\approx 6.0 \times 10^{-17}$ mol/mV at a gain ~30 over the Faraday cup at Nevada. Samples analyzed at Houston and New Mexico were irradiated at the Ford Nuclear Reactor at the University of Michigan while samples analyzed at Nevada were irradiated at the Nuclear Science Center at Texas A & M University. Measured $(^{40}Ar/^{39}Ar)_K$ values were 0.06884 ± 0.00039 (UH and NMT analyses) and 0.0505 ± 0.048 (UNLV analyses). Ca correction factors were $(^{39}Ar/^{37}Ar)_{Ca}$ = 0.0002311 ± 0.0000087 (UH and NMT analyses) and 0.0002771 ± 0.0000044 (UNLV analyses) while

$(^{39}Ar/^{37}Ar)_{Ca}$ = 0.0007173 ± 0.0000198 (UH and NMT analyses) and 0.0007433 ± 0.0000063 (UNLV analyses). J factors and calculated ages were determined using Fish Canyon Tuff 92-176 sanidine with an age of 27.9 Ma (Steven et al., 1967; Cebula et al., 1986). An error in J of 0.5% was used in all age calculations. Computer automated operation of UH and NMT laboratories and age calculations were completed using software written by A. Deino (University of California, Berkeley). The system at UNLV is operated using LabSPEC software written by B. Idelman (Lehigh University). All analytical errors are reported at the 1σ level.

A.4. Intercalibration of the $^{40}Ar/^{39}Ar$ dating laboratories

Intercalibration of the $^{40}Ar/^{39}Ar$ dating laboratories was accomplished by analyzing sample 31B. The UH data gave a mean age of 6.93 ± 0.09 Ma, NMT data gave a mean age of 6.85 ± 0.05 Ma while UNLV data gave a mean age of 6.98 ± 0.08 Ma (Table 7). These ages overlap at 1σ, thus $^{40}Ar/^{39}Ar$ ages from each laboratory are directly comparable.

A.5. $^{40}Ar/^{39}Ar$ data treatment

The homogeneity of analyzed crystal populations was assessed to allow identification of juvenile phenocrysts in cases where xenocrystic material may be present. Samples means and population standard deviations were calculated; any analyses outside of ± 2σ from the mean were excluded and a new mean calculated. Inverse variance weighted means (Young, 1962) of these refined data sets were calculated using analytical errors, then the 0.5% J factor error was added. Isochron ages were calculated using the York (1969) routine and a method outlined by Deino and Potts (1990) and Spell and Harrison (1993) with the mean square of weighted deviates (MSWD) cutoff value from Wendt and Carl (1991). If obtained, isochron ages are the preferred age of the unit. Some samples did not have a sufficient spread in radiogenic yield among analyses to define reliable isochrons. For these samples, the weighted mean was taken to represent the eruption age.

References

Aldrich, Jr., M.J., 1986. Tectonics of the Jemez lineament in the Jemez Mountains and Rio Grande rift. Journal of Geophysical Research 91, 1779–1798.

Bacon, C.R., Kurasawa, H., Delevaux, M.H., Kistler, R.W., Doe, B.R., 1981. Lead and strontium isotopic evidence for crustal interaction and compositional zonation in the source regions of Pleistocene basaltic and rhyolitic magmas of the Coso volcanic field, California. Contributions to Mineralogy and Petrology 85, 366–375.

Baldridge, W.S., Bartov, Y., Kron, A., 1983. Geologic map of the Rio Grande rift and southeast Colorado Plateau, New Mexico and Arizona. In: Riecker, R.E. (Ed.), Tectonics and Magmatism. American Geophysical Union, Washington, DC.

Barclay, J., Carroll, M., Houghton, B., Wolson, C., 1996. Pre-eruptive volatile content and degassing history of an evolving peralkaline volcano. Journal of Volcanology and Geothermal Research 74, 75–87.

Cebula, G.T., Kunk, M.J., Mehnert, H.H., Naeser, C.W., Obradovich, J.D., Sutter, J.F., 1986. The Fish Canyon Tuff, a potential standard for the $^{40}Ar/^{39}Ar$ and fission-track dating methods. Terra Cognita 6, 139–140.

Chen, W., Arculus, R.J., 1989. Geochemical and isotopic characteristics of lower crustal xenoliths, San Francisco volcanic field, Arizona, USA. Lithos 36, 203–225.

Deino, A.L., Potts, R., 1990. Single-crystal $^{40}Ar/^{39}Ar$ dating of the Olorgesailie Formation, southern Kenya rift. Journal of Geophysical Research 95, 8453–8470.

Doell, R.R., Dalrymple, G.B., Smith, R.L., Bailey, R.A., 1968. Paleomagnetism, potassium—argon ages, and geology of the rhyolites and associated rocks of the Valles Caldera. Memoirs Geol. Soc. Am. 116, 211–248.

Duffield, W.A., Dalrymple, G.B., 1990. The Taylor Creek Rhyolite of New Mexico: a rapidly emplaced field of lava domes and flows. Bulletin of Volcanology 52, 475–487.

Duffield, W.A., Ruiz, J., 1992. Compositional gradients in large reservoirs of silicic magma as evidenced by ignimbrites versus Taylor Creek Rhyolite lava domes. Contributions to Mineralogy and Petrology 110, 192–210.

Duffield, W.A., du Bray, E.A., 1990. Temperature, size, and depth of the magma reservoir of the Taylor Creek Rhyolite, New Mexico. American Mineralogist 75, 1059–1070.

Dunbar, N.W., Hervig, R.L., 1992. Volatile and trace element composition of melt inclusions from the lower Bandelier Tuff: implications for magma chamber processes and eruptive style. Journal of Geophysical Research 97, 15151–15170.

Dunker, K.E., Wolff, J.A., Harmon, R.S., Leat, P.T., Dickin, A.P., Thompson, R.N., 1991. Diverse mantle and crustal components in the lavas of the NW Cerros del Rio volcanic fields, Rio Grande rift, New Mexico. Contributions to Mineralogy and Petrology 108, 331–345.

Ellisor, R., 1995. Petrogenesis of the lavas and tuffs of the Keres Group, Jemez Mountains Volcanic Field. MS thesis, University of Texas, Arlington, TX (unpubl.).

Gardner, J.N., 1985. Tectonic and petrologic evolution of the Keres Group: implications for the development of the Jemez volcanic

field, New Mexico. PhD dissertation, University of California, Davis, CA (unpubl.).

Gardner, J.N., Goff, F., 1984. Potassium–argon dates from the Jemez volcanic field: implications for tectonic activity in the north-central Rio Grande rift. New Mexico Geological Society Guidebook 35, 75–81.

Gardner, J.N., Goff, F., Garcia, S., Hagan, R., 1986. Stratigraphic relations and lithologic variations in the Jemez volcanic field, New Mexico. Journal of Geophysical Research 91, 1763–1778.

Gay, K.R., Smith, G.A., 1996. Simultaneous phreatomagmatic and magmatic rhyolitic eruptions recorded in the late Miocene Peralta Tuff, Jemez Mountains, New Mexico. New Mexico Geological Society Guidebook 47, 243–250.

Goff, F., et al., 1989. Excursions 17B: volcanic and hydrothermal evolution of the Valles caldera and Jemez volcanic field. New Mexico Bureau of Mines and Mineral Resources Memoir 46, 381–434.

Goff, F., Gardner, J.N., Valentine, G., 1990. Geology of St Peter's Dome area, Jemez Mountains, New Mexico. New Mexico Bureau of Mines and Mineral Resources, geologic map, 69.

Golombek, M.P., 1981. Structural analysis of the Pajarito fault zone in the Española Basin of the Rio Grande rift, New Mexico. PhD dissertation, University of Massachusetts, Amherst, MA (unpubl.).

Golombek, M.P., 1983. Geology, structure, and tectonics of the Pajarito fault zone in the Española Basin of the Rio Grande rift, New Mexico. Geological Society of America Bulletin 94, 192–205.

Golombek, M.P., McGill, G.E., Brown, L., 1983. Tectonic and geologic evolution of the Española Basin, Rio Grande rift: structure, rate of extension, and relation to the state of stress in the Western US. Tectonophysics 94, 483–507.

Griggs, R.L., 1964. Geology and groundwater resources of the Los Alamos area, New Mexico. US Geologic Survey Water Supply Paper, 1753.

Hawkesworth, C.J., et al., 2000. Time scales of crystal fractionation in magma chambers—integrating physical, isotopic, and geochemical perspectives. Journal of Petrology 41, 991–1006.

Hervig, R.L., Dunbar, N.W., 1992. Cause of chemical zoning in the Bishop (California) and Bandelier (New Mexico) magma chambers. Earth and Planetary Science Letters 111, 97–108.

Izett, G.A., Obradovich, J.D., 1994. $^{40}Ar/^{39}Ar$ age constraints for the Jaramillo Normal Subchron and the Matayama–Brunhes geomagnetic boundary. Journal of Geophysical Research 99, 2925–2934.

Jacobs, J.W., Korotev, R.L., Blanchard, D.P., Haskins, L.A., 1977. A well tested procedure for instrumental neutron activation analysis of silicate rocks and minerals. Journal of Radioanalytical Chemistry 40, 93–114.

Justet, L., 1999. The geochronology and geochemistry of the Bearhead Rhyolite, Jemez volcanic field, New Mexico. MS thesis, University of Nevada, Las Vegas, NV (unpubl.).

Le Bas, M.J., Le Maitre, R.W., Streckeisen, A., Zanettin, B.A., 1986. Chemical classification of volcanic rocks based on the total alkali–silica diagram. Journal of Petrology 27, 745–750.

Lendlee, R.G., Smith, R.L., 1978. Map showing distribution, composition, and age of late Cenozoic volcanic centers in Arizona and New Mexico. US Geological Survey Miscellaneous Investigations Map I-1091-A.

Lindstrom, D.J., Korotev, R.L., 1982. TEABAGS—computer programs for instrumental neutron activation analysis. Journal of Radioanalytical Chemistry 70, 439–458.

Manley, K., 1976. The Late Cenozoic history of the Española Basin, New Mexico. PhD dissertation, University of Colorado, CO (unpubl.).

Manley, K., 1979b. Stratigraphy and structure of the Española Basin, Rio Grande rift, New Mexico. In Riecker, R.E. (Ed.), Rio Grande Rift: Tectonics and Magmatism. American Geophysical Union Special Publication, pp. 71–86.

McIntosh, W.C., Quade, J., 1995. $^{40}Ar/^{39}Ar$ geochronology of tephra layers in the Santa Fe Group, Española Basin, New Mexico. New Mexico Geological Society Guidebook 46, 279–287.

Nakamura, N., 1974. Determination of REE, Ba, Fe, Mg, Na, and K in carbonaceous and ordinary chondrites. Geochimica et Cosmochimica Acta 38, 757–775.

Norrish, K., Chappell, B.W., 1977. X-ray fluorescence spectrometry. In: Zussman, J. (Ed.), Physical Methods in Determinative Mineralogy. Academic Press, New York, pp. 201–272.

Norrish, K., Hutton, J.T., 1969. An accurate X-ray spectrographic method for the analysis of a wide range of geological samples. Geochimica et Cosmochimica Acta 33, 431–453.

Reid, M.R., Hart, S.R., Padovani, E.R., Wandless, G.A., 1989. Contribution of metapelitic sediments to the composition, heat production, and seismic velocity of the lower crust of southern New Mexico, USA. Earth and Planetary Science Letters 95, 367–381.

Reneau, S.L., Gardner, J.N., Forman, S.L., 1996. New evidence for the age of the youngest eruptions in the Valles caldera, New Mexico. Geology 24, 7–10.

Rudnick, R., Fountain, D., 1995. Nature and composition of the continental crust: a lower crustal perspective. Reviews of Geophysics 33, 267–309.

Self, S., Goff, F., Gardner, J., Wright, J., Kite, W., 1986. Explosive rhyolitic volcanism in the Jemez Mountains: vent locations, caldera development and relation to regional structure. Journal of Geophysical Research 91, 1779–1798.

Smith, R.L., Bailey, R.A., 1968. Resurgent cauldrons. Geological Society of America Memoir 116, 613–662.

Smith, G.A., Kuhle, A.J., 1998. Pattern of faulting, volcanism and sedimentation at the junction of the Jemez Mountains and Rio Grande rift, New Mexico. Geological Society of America Abstracts with Programs 30, 36.

Smith, R.L., Bailey, R.A., Ross, C.S., 1970. Geologic map of Jemez Mountains, New Mexico. US Geological Survey Miscellaneous Investigations Map I-571.

Sparks, R., Barclay, J., Jaupart, C., Mader, H., Phillips, J., 1994. Physical aspects of magma degassing. I. experimental and theoretical constraints on vesiculation. Reviews in Mineralogy 30, 413–445.

Spell, T.L., Harrison, T.M., 1993. $^{39}Ar/^{40}Ar$ geochronology of Post-Valles Caldera rhyolites, Jemez volcanic field, New Mexico. Journal of Geophysical Research 98, 8031–8051.

Spell, T.L., McDougall, I., Doulgeris, A.P., 1996. Cerro Toledo

Rhyolite, Jemez Volcanic Field, New Mexico: $^{40}Ar/^{39}Ar$ geochronology of eruptions between two caldera-forming events. Geological Society of America Bulletin 108, 1549–1566.

Steven, T.A., Mehnert, H.H., Obradovich, J.D., 1967. Age of volcanic activity in the San Juan Mountains, Colorado. United States Geological Survey Professional Paper, D47–D55.

Wallace, P.J., Anderson, A.T., Davis, A.M., 1999. Gradients in H_2O, CO_2, and exsolved gas in a large-volume silicic magma system: interpreting the record preserved in melt inclusion from the Bishop Tuff. Journal of Geophysical Research 104, 20097–20122.

Webster, J.D., Duffield, W.A., 1991. Volatiles and lithophile elements in Taylor Creek Rhyolite: constraints from glass inclusion analysis. American Mineralogist 76, 1628–1645.

Wendt, I., Carl, C., 1991. The statistical distribution of the mean squared weighted deviation. Chemical Geology 86, 275–285.

WohletGabriel, G., Goff, F., 1989. Temporal relations of volcanism and hydrothermal systems in two areas of the Jemez volcanic field, New Mexico. Geology 17, 986–989.

Wolff, J., Gardner, J.N., 1995. Is the Valles Caldera entering a new cycle of activity? Geology 23, 411–414.

York, D., 1969. Least squares fitting of a straight line with correlated errors. Earth and Planetary Science Letters 5, 320–324.

Young, H.D., 1962. Statistical Treatment of Experimental Data. McGraw Hill, New York.